What About Manganese? Toward Rocking Chair Aqueous Mn-Ion Batteries

ACS Energy LETTERS

http://pubs.acs.org/journal/aelccp

What About Manganese? Toward Rocking Chair Aqueous Mn-Ion Batteries

Amey Nimkar, Munseok S. Chae, Shianlin Wee, Gil Bergman, Bar Gavriel, Meital Turgeman, Fyodor Malchik, Mikhael D. Levi, Daniel Sharon, Maria R. Lukatskaya, Netanel Shpigel,* and Daniel Mandler

Cite This: *ACS Energy Lett.* 2022, 7, 4161−4167

Read Online

ACCESS | Metrics & More | Article Recommendations | Supporting Information

ABSTRACT: The emerging interest in aqueous rechargeable batteries has led to significant progress in the development of next-generation electrolytes and electrode materials enabling reversible and stable insertion of various multivalent ions into the electrode's bulk. Yet, despite its abundance, high salt solubility, and small ionic radius, the use of manganese ions for energy storage purposes has not received sufficient attention. Herein, we present the use of Mo_6S_8 (Chevrel phase) as an anode for Mn^{2+} insertion. By careful optimization of the electrolyte solution, high-capacity values exceeding 90 mAh/g and long-term stability (more than 1500 cycles) have been obtained. Based on in situ XRD analysis, the charging mechanism and the associated structural changes occurring during Mn^{2+} insertion have been carefully studied. Finally, we demonstrate for the first time a rocking chair aqueous Mn-ion battery comprising a Chevrel anode and NiHCF cathode.

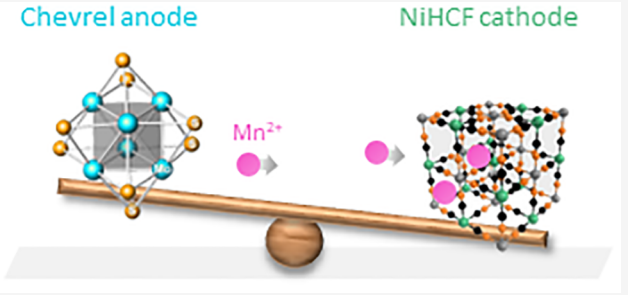

The search for viable alternatives to Li-based batteries has led to extensive research efforts toward utilization of other cations for electrochemical energy storage.[1,2] For grid-level energy storage in MWh to TWh scales, usage of flammable organic electrolytes poses a major concern. Meanwhile, aqueous electrolytes are safe and environmentally friendly and therefore serve as an attractive alternative.[3] The need for safe batteries for large energy storage leads to the accelerated development of novel aqueous electrolytes in which hydrogen and oxygen evolution are suppressed as a result of decreased water activity or/and formation of the solid electrolyte interface layer.[4] Such optimizations lead to realization of aqueous electrolytes that have an extended potential window of up to 4 V,[5] allowing for the usage of various anode and cathode materials that have intercalation/deintercalation potentials outside the thermodynamic stability window of water.[6] Given the need for abundant and cheap battery materials, substantial research efforts have been directed toward post-lithium ion batteries,[7] particularly Na-ion[8] and K-ion;[9] meanwhile, with respect to water-based batteries, most of the studies are focused on Zn-metal batteries.[10] In the search for further potential transition metals (TM), electrolytes based on precious (Au, Pt, Ag), low abundant (Co, Ni) toxic heavy metals (Hg, Pb, Cd, Cr), and poor soluble cations (Ti) are obviously less attractive. Manganese (Mn) on the other hand is an abundant (about 12 times more abundant than Zn[11]), safe, and inexpensive element,[12] and its salts are highly soluble in water. These advantageous characteristics make Mn an ideal ion for large-scale energy storage applications. As the ionic radius of Mn^{2+} is only slightly larger than that of Zn^{2+} (i.e., 0.81 Å vs 0.74 Å respectively),[13] many Zn-ion hosting compounds such as Prussian blue analogs, V_2O_5, MnO_2, etc. may well accommodate insertion of Mn ions as well.[14]

Despite the enormous potential of aqueous Mn-based batteries, the use of Mn^{2+} as a charge carrier cation in aqueous batteries appears to have received limited attention compared to zinc. Only recently an Mn-metal battery paired with V_2O_5 and benzoquinone as possible cathodes was reported by Bi et al.[15] However, the electrochemical stripping and deposition process of the Mn metal anode was not described in depth in the publication, raising questions about the reversibility of the system and its charge storage mechanism. As the standard reduction potential of Mn/Mn^{2+} is significantly more negative

Received: October 3, 2022
Accepted: October 19, 2022
Published: October 27, 2022

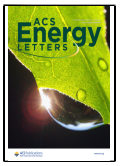

https://doi.org/10.1021/acsenergylett.2c02242
ACS Energy Lett. 2022, 7, 4161−4167

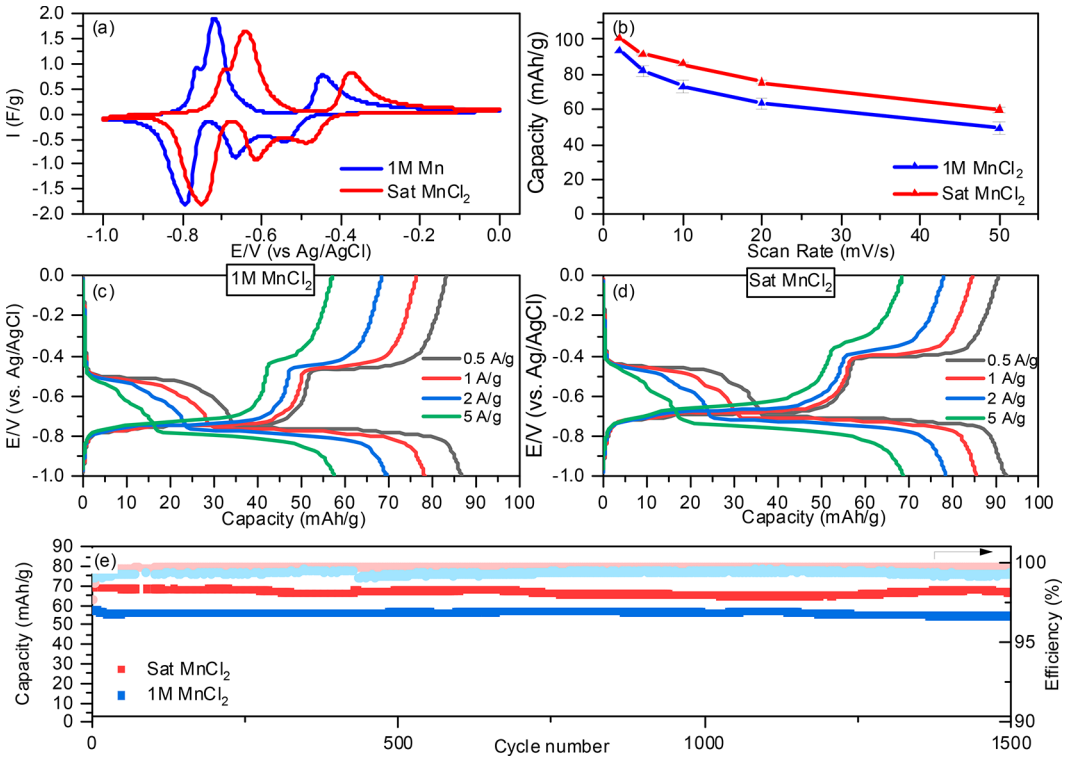

Figure 1. Electrochemical studies of Mn-ion intercalation into Chevrel electrodes in 1 M and saturated $MnCl_2$. (a) Cyclic voltammetry profiles collected at 2 mV/s. (b) Capacity vs scan rate plot. The error bars were calculated based on three independent measurements. The GCD profiles of 1 M and saturated $MnCl_2$ are shown in panels (c) and (d), respectively. (e) Long-term performance of Mo_6S_8 measured at 5 A/g.

than Zn/Zn^{2+} (i.e., −1.19 V compared to −0.76 V, both vs SHE), Mn-metal batteries can potentially offer attractive energy densities that are higher than Zn-based systems. In practice, however, with such a low reduction potential of Mn^{2+} in conventional aqueous electrolytes, a concurrent hydrogen evolution reaction (HER) is unavoidable due to parasitic water decomposition, resulting in poor reversibility of the Mn plating process. To address this issue, Yang et al. recently suggested using a modified electrolyte solution containing 0.6 M $MnSO_4$, 2.5 M $NaClO_4$, and 1.4 M glycine.[16] The latter components are introduced to increase the ionic conductivity of the electrolyte ($NaClO_4$) and suppress the water activity in the solution, thus increasing the overpotential for HER. Yet, despite the improved performance, the cell is unsuitable for practical applications, mostly due to the poor reversibility of the Mn anode. Considering the complexity of the Mn deposition/stripping process and its poor efficiency,[17] new anodes that allow the reversible insertion of Mn ions should be developed. Herein we demonstrate that Mo_6S_8 (Chevrel) can be used as an effective anode material for Mn-ion intercalation-based batteries. Using saturated $MnCl_2$ solution as an electrolyte, high capacity values and promising long-term cycling performance of the Chevrel anodes have been shown. Further mechanistic insights related to the Mn intercalation process including its migration pathways, the associated activation energies, and the possibility of co-insertion of protons to the Chevrel host structure were provided using in situ XRD. Finally, a rocking chair Mn-ion battery comprising Chevrel anode and nickel hexacyanoferrate (NiHCF) cathodes was demonstrated.

In search for potential anode materials capable of reversible insertion of Mn ions, we evaluated the use of the Chevrel phase (Mo_6S_8). While Chevrel-based electrodes were predominantly studied as cathodes for Mg-ion batteries,[18] its unique structure allows fast and reversible insertion of various transition metal cations including Zn(II),[19] Ni(II), and Co(II).[20] The possibility of intercalation of Mn(II) ions into the Chevrel structure was discovered more than three decades ago;[21] however, to the best of our knowledge, the use of Chevrel electrodes for Mn-ion batteries has never been reported.

The Chevrel phase was made according to prior reports.[22] As can be seen, the synthesized Chevrel contains micron-sized aggregates composed of small nanometric particles with an average dimension of 100 nm (Figure S1a). The XRD pattern of the Chevrel corresponds to a rhombohedral crystal structure (Figure S1b). The electrochemical insertion of Mn ions into the Chevrel electrodes was evaluated in 1 M and saturated (6.97 M) $MnCl_2$ solutions. The potential stability window of both diluted and saturated solution was first measured on bare grafoil substrate. As shown in Figure S2, a stable electrochemical window was obtained upon scanning from −1 V to 0.95 V in both electrolyte solutions. Interestingly, for the concentrated electrolyte, the potential window can be extended up to −1.4 V, whereas below this voltage, Mn ions are partially reduced to metallic manganese followed by H_2 generation and formation of $Mn(OH)_2$ (see zone ii in Figure S2). In contrast in the diluted solution, the Mn deposition potential can not be approached at this range, and completely irreversible currents resulting from H_2 formation were observed. The formation of $Mn(OH)_2$ on the cathodic side facilitates irreversible formation of $Mn(OH)_2$ at the relatively low anodic potentials (zone (iii)) indicated by a pronounced oxidation wave at ∼0.5 V (vs Ag/AgCl). Finally, beyond 1.05

https://doi.org/10.1021/acsenergylett.2c02242
ACS Energy Lett. 2022, 7, 4161−4167

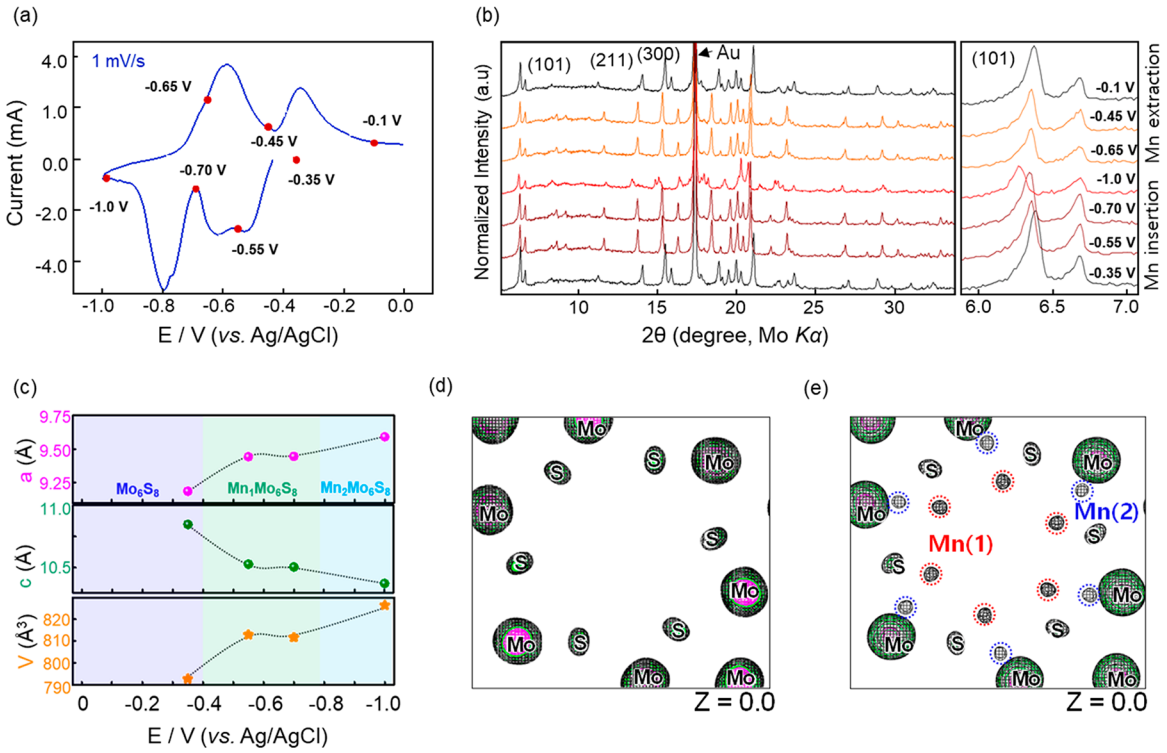

Figure 2. (a) Cyclic voltammograms of Mn(II) intercalation into Mo_6S_8. (b) *In-situ* XRD data for each CV potential are marked in (a). (c) Evolution of the volume and unit cell parameters during the discharge process. Calculated Fourier maps for (d) pristine Mo_6S_8 powder and (e) electrochemically manganese inserted $Mn_2Mo_6S_8$ at the (*x*, *y*, 0) layer.

V, the Cl_2 evolution reaction takes place. Nevertheless, working in the stable potential regime (zone I in Figure S2) guarantees a a suitable operating range.

Considering the above, the cyclic voltammogram (CV) of the Chevrel electrodes in both 1 M and saturated electrolytes solutions is shown in Figure 1a. As can be seen, the insertion process of Mn^{2+} into the Mo_6S_8 host is characterized by three well-resolved redox peaks. A "Nernstian type" shift of ∼50 mV toward positive potentials is observed when switching from diluted to saturated electrolytes. Similar to other divalent cations, the insertion of Mn^{2+} into Chevrel structure involves four-electron transfer accompanied by intercalation of two Mn(II) ions, according to the following equation:[23]

$$2Mn^{2+} + 4\bar{e} + Mo_6S_8 \rightarrow Mn_2Mo_6S_8$$

As the Chevrel structure has two tetrahedral sites accessible for cation insertion, the intercalation of TM ions into Chevrel is expected to occur via multiple steps.[24] The peaks at high potentials are related to the occupation of the inner sites in the Mo_6S_8 structure, while insertion of cations into the outer sites occurs at more negative potentials. Interestingly, unlike intercalation of Mg[25] or Zn[26] cations which is expressed by two well-defined redox peaks, intercalation of Mn^{2+} into the Chevrel structure appears to be more complex. Such phenomena might be related to possible changes in the oxidation state of the Mn(II) that occur at various intercalation stages[23] or to a rearrangement of the inserted ions in the two possible insertion sites (i.e., hoping from cavity 1 to cavity 2 as will be further discussed) due to electrostatic repulsions between the intercalated Mn ions.[27] Clearly, further in-depth studies are needed to reveal the true origin of this behavior.

Figure 1b depicts the capacity dependence on charging rates (the corresponding CV profiles are shown in Figure S3). Galvanostatic charge−discharge (GCD) profiles collected at 0.5 A/g (Figure 1c,d) reveal experimental capacity values of 93 ± 1.4 mAh/g in concentrated $MnCl_2$ electrolytes, while a lower value of 86 ± 3.3 mAh/g was measured in the diluted electrolytes. More pronounced capacity differences were observed at the highest current density (5 A/g) where the value of 68 ± 1.4 mAh/g was obtained in the saturated electrolyte, while only 57 ± 3.2 mAh/g was detected in 1 M $MnCl_2$. Nevertheless, as shown in Figure 1e, excellent long-term cycling stability was observed in both saturated and diluted solutions as expressed by a capacity retention of more than 96% after 1500 cycles and high Coulombic efficiencies (>99.3%).

Importantly, application of low current densities allows approaching the theoretical capacity values of $Mn_2Mo_6S_8$, viz. 113 mAh/g as shown in Figure S4. Further energy-dispersive X-ray spectroscopy (EDS) of the cycled Chevrel electrodes reveals the presence of Mn in the charged (−1 V) samples but not in the discharge (0 V) anodes; see Figure S5.

The difference in experimental capacity values in 1 M and saturated electrolytes raises the question of the origin of the enhanced capacity in the saturated $MnCl_2$ solution. As the ionic conductivity of the dilute solution is higher than that of the saturated solution (i.e., 48 mS/cm vs 37 mS/cm for 1 M and saturated solution, respectively), this effect cannot be attributed to the kinetics of the Mn ion intercalation process. Therefore, we considered another hypothesis that higher capacity in saturated $MnCl_2$ might be attributed to co-intercalation of protons into the Chevrel due to the acidic nature of these solutions (pH = 1.4 for saturated vs pH = 4 for 1 M $MnCl_2$). To test this, we adjusted the pH of the diluted electrolyte by adding a calculated amount of HCl (0.013 M) into a 1 M $MnCl_2$ solution to achieve a pH value roughly

https://doi.org/10.1021/acsenergylett.2c02242
ACS Energy Lett. 2022, 7, 4161−4167

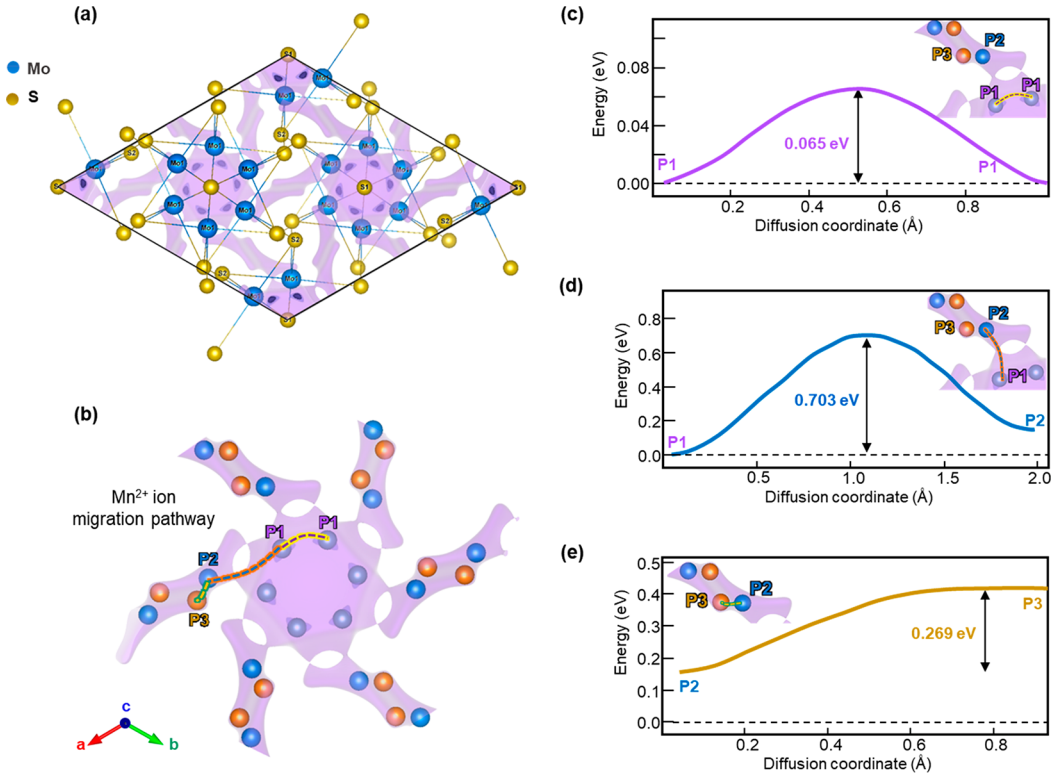

Figure 3. (a) Calculated migration paths for the manganese ion are shown along the *c*-axis direction. (b) Manganese migration unit and diffusion points. The calculated migration barriers and diffusion paths for the manganese ion shown in (c) P1−P1, (d) P1−P2, (e) P2−P3 path.

comparable to that of the saturated solutions. The GCD profiles of the low concentration cells that were acidified (comparable to that of the saturated solutions). The GCD profiles of the low concentration cells that were acidified (Figure S6a) show that the capacity values of the Chevrel electrode were increased to values comparable to those of the saturated electrolytes. Furthermore, the performance of the Mo_6S_8 in 0.013 M HCl electrolytes clearly indicates the insertion of protons into the Chevrel phase. This is evident from the well-expressed voltage plateaus and reversible redox peaks in the GCD and CV plots shown in Figure S6b,c, respectively. To the best of our knowledge, the possibility of proton intercalation into Chevrel has never been reported. As can be seen from Figure S7, electrochemical cycling of the Chevrel in highly acidic conditions (e.g., 0.5 M HCl) results in significant water splitting that takes place at potentials well before the proton intercalation; therefore, insertion of protons into Chevrel can be achieved only in diluted acids.

Further understanding of the manganese intercalation mechanism was accomplished by *in-situ* XRD measurements. The XRD measurements were taken from a selected point upon the negative and the positive scanning potentials of the CV measurement (see Figure 2a). The corresponding changes in the XRD patterns are shown in Figure 2b. As can be seen, a gradual shift toward lower angles during Mn insertion was identified. The peaks were shifted back to their original position upon Mn extraction (charging) process. Based on the observed shift, a reversible expansion/contraction during the Mn insertion/extraction process of 4.41% was calculated for *a* unit cell parameters, whereas the unit cell parameter *c* decreased by 4.37%, and the total unit cell volume expanded by 4.26% after Mn insertion (Figure 2e). Detailed information on unit cell evolutions can be found in Table S1. The pristine Mo_6S_8 and manganese inserted phases were further analyzed by X-ray Rietveld refinement (Figure S8; Figure 2c,d) and electron density maps (Figure 2d,e). From the obtained electron density map, one can see that the manganese ions are equally distributed inside the inner cavity (denoted as Mn1) and outer cavity (Mn2) both comprising six equivalent tetrahedral sites as illustrated in Figure S9.

The manganese migration pathways (purple colored zones) along the *c*-axis are shown in Figure 3a,b. In general, the diffusion of the metal ions in the Chevrel structure occurs via two competing transport pathways viz. circular motion of the ion within six equivalent tetrahedra sites of cavity 1 (denoted as P1−P1 in Figure 3b) and diffusion between adjacent cavities (usually from P1 to P2 through P3).[28] As depicted in Figure 3c−e, the lowest activation barrier was found for P1 to P1 (0.065 eV). As the distance between two neighboring inner sites is significantly shorter than the distance between the inner and the outer sites (i.e., M1 and M2, see Figure S9) and due to the stronger repulsion interactions of the Mn−Mo in the outer sites, the inserted Mn atom will first occupy the first cavity. Unless higher polarization to more negative potential is applied, the Mn ions will move in a circular motion in the inner ring.[29] Indeed, higher activation energy was calculated for Mn motion from P1−P2 (0.269 eV), while the highest migration barrier was calculated for Mn diffusion from P2−P3 (0.703 eV). As this pathway is less favorable from an energetic point of view, it has a major influence on the ion's progressive diffusion.

In a similar way, we have calculated the proton cation migration in the Chevrel lattice. Figure S10a,b presents the migration pathways through the *ab*-plane and along the *c*-axis.

https://doi.org/10.1021/acsenergylett.2c02242
ACS Energy Lett. 2022, 7, 4161−4167

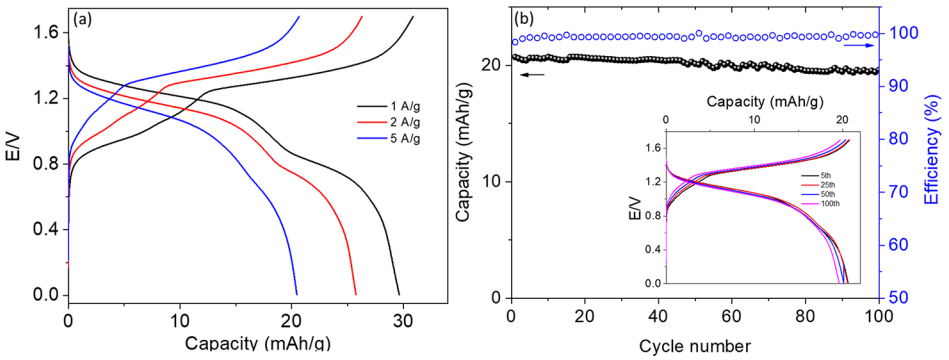

Figure 4. Electrochemical behavior of a rocking chair Mn-ion battery. (a) GCD profiles at different current densities, (b) long-term stability of a full cell comprising Mo_6S_8 anode and NiHCF cathode

Due to their smaller size, proton intercalation into the Chevrel matrix is defined by a lower activation barrier (0.230 eV) than manganese insertion (0.703 eV) (see Figure S10d,e). The possible proton sites in the Chevrel phase are suggested based on the lowest energy diffusion pathways as depicted in Figure S10.

Encouraged by the excellent performance of the anode side, our further efforts were directed toward finding a suitable cathode to enable the reversible insertion of Mn ions. Although the use of V_2O_5 as an insertion cathode for Mn-ion was recently proposed,[30,31] its potential operation range is wide, spreading over 2 V as can be seen from GCD profiles (see Figure S11) making this cathode not practical. In the search for a more suitable cathode material, the use of NiHCF was evaluated. Detailed information about the synthesis of the NiHCF, XRD, and SEM images can be found in the Experimental Section and in Figure S12. Using saturated $MnCl_2$ electrolyte, capacity values of 43 mAh/g at 0.5A/g and 24 mAh/g at 5A/g were observed. Yet, a relatively fast capacity fading of 63% was observed throughout 500 cycles (Figure S13).

The electrochemical performance of the full cell comprising a Chevrel anode and a NiHCF cathode is presented in Figure 4. As seen from the GCD profiles in Figure 4a, an average voltage of 1.2 V and overall capacity of ∼30 mAh/g, 25 mAh/g, and 20 mAh/g (based on the mass of both electrodes) were measured at 1, 2, and 5 A/g, respectively. During 100 cycles, 92% of the initial capacity was preserved, while no significant changes in the voltage profiles were identified (see Figure 4b).

As can be seen in Figure 4b, the stability of the full cell still poses a challenge. Clearly, as the stability of the NiHCF cathode in the half-cell configurations was significantly lower than that of the Chevrel, the rapid fading of the full cell can be attributed to the degradation on the cathode side. As the performance of Prussian blue analog structures are highly affected by the synthesis conditions and their compositions,[32] future synthesis efforts may help to improve cycling stability of the NiHCF cathodes.

In summary, the use of Mo_6S_8 as an anode allowing the reversible Mn-ion insertion from aqueous electrolytes was demonstrated. By application of *in-situ* XRD, the migration pathways and the associated diffusion energy barriers of both Mn and protons inside the Chevrel structure have been revealed. Unlike metallic Mn which raises significant difficulties for practical utilization in aqueous and organic electrolyte solutions,[33] the use of Chevrel as an anode enables excellent Mn-ion storage capacities and cycling stability, making it an attractive anode candidate for aqueous Mn-ion batteries. Finally, a rocking chair Mn-ion battery comprising a Chevrel anode and NiHCF cathode was successfully demonstrated for the first time. Regarding the cathode side, further investigations are needed to find suitable electrode materials with higher capacity and better stability. Nevertheless, as the field of Mn-ion batteries is at its infancy, we strongly believe that this study will promote further investigations of the anode and cathode materials for Mn-based energy storage applications.

■ ASSOCIATED CONTENT

Supporting Information

The Supporting Information is available free of charge at https://pubs.acs.org/doi/10.1021/acsenergylett.2c02242.

Synthesis procedures and characterization of Chevrel phase and NiHCF materials, electrode preparations, in situ XRD measurement details, supporting electrochemical experiments including proton intercalation using acid (PDF)

■ AUTHOR INFORMATION

Corresponding Author

Netanel Shpigel − *Institute of Chemistry, The Hebrew University of Jerusalem, Jerusalem 9190401, Israel*; Email: nshpigel@gmail.com

Authors

Amey Nimkar − *Department of Chemistry and BINA − BIU Centre for Nanotechnology and Advanced Materials, Bar-Ilan University, Ramat-Gan 5290002, Israel*

Munseok S. Chae − *Department of Chemistry and BINA − BIU Centre for Nanotechnology and Advanced Materials, Bar-Ilan University, Ramat-Gan 5290002, Israel*; orcid.org/0000-0002-4450-0846

Shianlin Wee − *Electrochemical Energy Systems Laboratory, Department of Mechanical and Process Engineering, ETH Zurich, 8092 Zurich, Switzerland*

Gil Bergman − *Department of Chemistry and BINA − BIU Centre for Nanotechnology and Advanced Materials, Bar-Ilan University, Ramat-Gan 5290002, Israel*

Bar Gavriel − *Department of Chemistry and BINA − BIU Centre for Nanotechnology and Advanced Materials, Bar-Ilan University, Ramat-Gan 5290002, Israel*

Meital Turgeman − *Department of Chemistry and BINA − BIU Centre for Nanotechnology and Advanced Materials, Bar-Ilan University, Ramat-Gan 5290002, Israel*

https://doi.org/10.1021/acsenergylett.2c02242
ACS Energy Lett. 2022, 7, 4161−4167

Fyodor Malchik − *Center of Physical-Chemical Methods of Research and Analysis, al-Farabi Kazakh National University, Almaty 050012, Kazakhstan*
Mikhael D. Levi − *Department of Chemistry and BINA − BIU Centre for Nanotechnology and Advanced Materials, Bar-Ilan University, Ramat-Gan 5290002, Israel*
Daniel Sharon − *Institute of Chemistry, The Hebrew University of Jerusalem, Jerusalem 9190401, Israel*
Maria R. Lukatskaya − *Electrochemical Energy Systems Laboratory, Department of Mechanical and Process Engineering, ETH Zurich, 8092 Zurich, Switzerland;* orcid.org/0000-0002-2794-4322
Daniel Mandler − *Institute of Chemistry, The Hebrew University of Jerusalem, Jerusalem 9190401, Israel;* orcid.org/0000-0003-2490-1084

Complete contact information is available at: https://pubs.acs.org/10.1021/acsenergylett.2c02242

Notes

The authors declare no competing financial interest.

■ ACKNOWLEDGMENTS

N.S. acknowledges the Israel Academy of Sciences and Humanities for its financial support. This research is partially funded by the Science Committee of the Ministry of Education and Science of the Republic of Kazakhstan (Grant No. AP08856725). M.R.L. acknowledges support from the ReMaP project funded by the Swiss Federal Office of Energy under Contract SI/501810-01 and the ETH Foundation.

■ REFERENCES

(1) Liang, Y.; Dong, H.; Aurbach, D.; Yao, Y. Current Status and Future Directions of Multivalent Metal-Ion Batteries. *Nature Energy 2020 5:9* **2020**, *5* (9), 646−656.
(2) Tian, Y.; Zeng, G.; Rutt, A.; Shi, T.; Kim, H.; Wang, J.; Koettgen, J.; Sun, Y.; Ouyang, B.; Chen, T.; Lun, Z.; Rong, Z.; Persson, K.; Ceder, G. Promises and Challenges of Next-Generation "beyond Li-Ion" Batteries for Electric Vehicles and Grid Decarbonization. *Chem. Rev.* **2021**, *121* (3), 1623−1669.
(3) Dong, C.; Xu, F.; Chen, L.; Chen, Z.; Cao, Y. Design Strategies for High-Voltage Aqueous Batteries. *Small Struct* **2021**, *2* (7), 2100001.
(4) Martins, V. L.; Torresi, R. M. Water-in-Salt Electrolytes for High Voltage Aqueous Electrochemical Energy Storage Devices. *Curr. Opin Electrochem* **2020**, *21*, 62−68.
(5) Yang, C.; Chen, J.; Qing, T.; Fan, X.; Sun, W.; von Cresce, A.; Ding, M. S.; Borodin, O.; Vatamanu, J.; Schroeder, M. A.; Eidson, N.; Wang, C.; Xu, K. 4.0 V Aqueous Li-Ion Batteries. *Joule* **2017**, *1* (1), 122−132.
(6) Lukatskaya, M. R.; Feldblyum, J. I.; Mackanic, D. G.; Lissel, F.; Michels, D. L.; Cui, Y.; Bao, Z. Concentrated Mixed Cation Acetate "Water-in-Salt" Solutions as Green and Low-Cost High Voltage Electrolytes for Aqueous Batteries. *Energy Environ. Sci.* **2018**, *11*, 2876.
(7) Tian, Y.; Zeng, G.; Rutt, A.; Shi, T.; Kim, H.; Wang, J.; Koettgen, J.; Sun, Y.; Ouyang, B.; Chen, T.; Lun, Z.; Rong, Z.; Persson, K.; Ceder, G. Promises and Challenges of Next-Generation "beyond Li-Ion" Batteries for Electric Vehicles and Grid Decarbonization. *Chem. Rev.* **2021**, *121* (3), 1623−1669.
(8) Liu, M.; Ao, H.; Jin, Y.; Hou, Z.; Zhang, X.; Zhu, Y.; Qian, Y. Aqueous Rechargeable Sodium Ion Batteries: Developments and Prospects. *Mater. Today Energy* **2020**, *17*, 100432.
(9) Wang, Y.; Liu, D.; Sun, M.; Liu, J. Recent Progress in Electrode Materials for Aqueous Sodium and Potassium Ion Batteries. *Mater. Chem. Front* **2021**, *5* (20), 7384−7402.
(10) Ruan, P.; Liang, S.; Lu, B.; Fan, H. J.; Zhou, J. Design Strategies for High-Energy-Density Aqueous Zinc Batteries. *Angew. Chem., Int. Ed.* **2022**, *61* (17), No. e202200598.
(11) Haynes, W. M.*CRC Handbook of Chemistry and Physics*, 97th ed.; CRC Handbook of Chemistry & Physics, 2016; p 2670.
(12) Xie, C.; Li, T.; Deng, C.; Song, Y.; Zhang, H.; Li, X. A Highly Reversible Neutral Zinc/Manganese Battery for Stationary Energy Storage. *Energy Environ. Sci.* **2020**, *13* (1), 135−143.
(13) Heimann, J.; Morrow, L.; Anderson, R. E.; Barron, A. R. Understanding the Relative Binding Ability of Hydroxyfullerene to Divalent and Trivalent Metals. *Dalton Transactions* **2015**, *44* (9), 4380−4388.
(14) Li, C.; Zhang, X.; He, W.; Xu, G.; Sun, R. Cathode Materials for Rechargeable Zinc-Ion Batteries: From Synthesis to Mechanism and Applications. *J. Power Sources* **2020**, *449*, 227596.
(15) Bi, S.; Wang, S.; Yue, F.; Tie, Z.; Niu, Z. A Rechargeable Aqueous Manganese-Ion Battery Based on Intercalation Chemistry. *Nature Communications 2021 12:1* **2021**, *12* (1), 1−11.
(16) Yang, Q.; Qu, X.; Cui, H.; He, X.; Shao, Y.; Zhang, Y.; Guo, X.; Chen, A.; Chen, Z.; Zhang, R.; Kong, D.; Shi, Z.; Liu, J.; Qiu, J.; Zhi, C. Rechargeable Aqueous Mn Metal Battery Enabled by Inorganic-Organic Interfaces. *Angew. Chem., Int. Ed.* **2022**, DOI: 10.1002/anie.202206471.
(17) Padhy, S. K.; Patnaik, P.; Tripathy, B. C.; Ghosh, M. K.; Bhattacharya, I. N. Electrodeposition of Manganese Metal from Sulphate Solutions in the Presence of Sodium Octyl Sulphate. *Hydrometallurgy* **2016**, *165*, 73−80.
(18) Levi, E.; Gofer, Y.; Vestfreed, Y.; Lancry, E.; Aurbach, D. Cu2Mo6S8 Chevrel Phase, a Promising Cathode Material for New Rechargeable Mg Batteries: A Mechanically Induced Chemical Reaction. *Chemistry of materials* **2002**, *14* (6), 2767−2773.
(19) Cheng, Y.; Luo, L.; Zhong, L.; Chen, J.; Li, B.; Wang, W.; Mao, S. X.; Wang, C.; Sprenkle, V. L.; Li, G.; Liu, J. Highly Reversible Zinc-Ion Intercalation into Chevrel Phase Mo6S8 Nanocubes and Applications for Advanced Zinc-Ion Batteries. *ACS Appl. Mater. Interfaces* **2016**, *8* (22), 13673−13677.
(20) Guyot, E.; Seghir, S.; Lecuire, J. M.; Boulanger, C.; Levi, M. D.; Shilina, Yu.; Dargel, V.; Aurbach, D. Mo 6 S 8 Electrochemical Transfer Junction for Selective Extraction of Co 2+ -Ions from Their Mixture with Ni 2+ -Ions. *J. Electrochem. Soc.* **2013**, *160* (3), A420−A425.
(21) Boulanger, C.; Lecuire, J. M. Insertion Electrochimique de Nickel et de Manganese Dans Les Chalcogenures Mo6S8 et Mo6Se8. *Electrochim. Acta* **1987**, *32* (2), 345−348.
(22) Malchik, F.; Shpigel, N.; Levi, M. D.; Mathis, T. S.; Mor, A.; Gogotsi, Y.; Aurbach, D. Superfast High-Energy Storage Hybrid Device Composed of MXene and Chevrel-Phase Electrodes Operated in Saturated LiCl Electrolyte Solution. *J. Mater. Chem. A Mater.* **2019**, *7* (34), 19761−19773.
(23) Levi, E.; Gershinsky, G.; Aurbach, D.; Isnard, O. Crystallography of Chevrel Phases, MMo6T8 (M= Cd, Na, Mn, and Zn, T= S, Se) and Their Cation Mobility. *Inorg. Chem.* **2009**, *48* (18), 8751−8758.
(24) Mei, L.; Xu, J.; Wei, Z.; Liu, H.; Li, Y.; Ma, J.; Dou, S. Chevrel Phase Mo6T8 (T = S, Se) as Electrodes for Advanced Energy Storage. *Small* **2017**, *13* (34), 1701441.
(25) Levi, M. D.; Lancry, E.; Gizbar, H.; Lu, Z.; Levi, E.; Gofer, Y.; Aurbach, D. Kinetic and Thermodynamic Studies of Mg2+ and Li+ Ion Insertion into the Mo6 S 8 Chevrel Phase. *J. Electrochem. Soc.* **2004**, *151* (7), A1044−A1051.
(26) Cheng, Y.; Luo, L.; Zhong, L.; Chen, J.; Li, B.; Wang, W.; Mao, S. X.; Wang, C.; Sprenkle, V. L.; Li, G.; Liu, J. Highly Reversible Zinc-Ion Intercalation into Chevrel Phase Mo6S8 Nanocubes and Applications for Advanced Zinc-Ion Batteries. *ACS Appl. Mater. Interfaces* **2016**, *8* (22), 13673−13677.
(27) Geng, L.; Scheifers, J. P.; Zhang, J.; Bozhilov, K. N.; Fokwa, B. P. T.; Guo, J. Crystal Structure Transformation in Chevrel Phase Mo6S8 Induced by Aluminum Intercalation. *Chem. Mater.* **2018**, *30* (23), 8420−8425.

(28) Levi, E.; Gershinsky, G.; Aurbach, D.; Isnard, O. Crystallography of Chevrel Phases, MMo6T8 (M = Cd, Na, Mn, and Zn, T = S, Se) and Their Cation Mobility. *Inorg. Chem.* **2009**, *48* (18), 8751−8758.
(29) Levi, E.; Lancry, E.; Mitelman, A.; Aurbach, D.; Isnard, O.; Djurado, D. Phase Diagram of Mg Insertion into Chevrel Phases, MgxMo 6T8 (T = S, Se). 2. THe Crystal Structure of Triclinic MgMo6Se8. *Chem. Mater.* **2006**, *18* (16), 3705−3714.
(30) Bi, S.; Wang, S.; Yue, F.; Tie, Z.; Niu, Z. A Rechargeable Aqueous Manganese-Ion Battery Based on Intercalation Chemistry. *Nature Communications 2021 12:1* **2021**, *12* (1), 1−11.
(31) Bi, S.; Zhang, Y.; Deng, S.; Tie, Z.; Niu, Z.Proton-Assisted Aqueous Manganese-Ion Battery Chemistry. *Angewandte Chemie - International Edition***2022**, *61* (17). DOI: 10.1002/anie.202200809.
(32) Wang, B.; Han, Y.; Wang, X.; Bahlawane, N.; Pan, H.; Yan, M.; Jiang, Y. Prussian Blue Analogs for Rechargeable Batteries. *iScience* **2018**, *3*, 110−133.
(33) Lu, J.; Dreisinger, D.; Glück, T. Manganese Electrodeposition — A Literature Review. *Hydrometallurgy* **2014**, *141*, 105−116.

https://doi.org/10.1021/acsenergylett.2c02242
ACS Energy Lett. 2022, 7, 4161−4167